# Impulse scattering from clouds of acoustically coupled gas bubbles in fluids

M. P. Raveau[a] and C. Escauriaza[b]

Department of Hydraulic and Environmental Engineering

Pontificia Universidad Católica de Chile,

Avenida Vicuña Mackenna 4860, Santiago, Chile

C. N. Dolder [c]and P. S. Wilson[d]

Department of Mechanical Engineering and Applied Research Laboratories

The University of Texas at Austin, Austin, Texas 78712

C. Feuillade[e]

Institute of Physics, Pontificia Universidad Católica de Chile,

Avenida Vicuña Mackenna 4860, Santiago, Chile

[a]e-mail: mpraveau@uc.cl

[b]e-mail: cescauri@ing.puc.cl

[c]e-mail: dolder@utexas.edu

[d]e-mail: pswilson@mail.utexas.edu

[e]e-mail: chris.feuillade@gmail.com

**Abstract**

To calculate the impulse response of a bubble cloud in a compressible medium we develop a methodology that incorporates multiple scattering effects between bubbles, and coherent interactions of their individual scattered fields. This method is based on the perturbation theory, and provides for an approximate solution formulated by adding a perturbation to the mathematical description of a linear problem. The solution is defined as a power series, where the first term of the expansion corresponds to the solution of a linear uncoupled equation. The convergence of the expansion is determined by the parameters of the physical bubbles, and the acoustic interactions. The model is successfully applied to describe experimental measurements of a model bubble cloud response in a shallow fresh-water environment.

# I  Introduction

Sound propagation in the ocean has been a topic of great importance since the middle of the last century. While light is typically absorbed within a few meters in the water column, sound can propagate long distances with relatively little attenuation. Therefore, acoustic methods have been widely used as a tool to investigate the ocean. Originally developed for military purposes, ocean acoustics has expanded its scope and has been used for the exploration and mapping of the seabed, the remote sensing of fish schools, and the study of marine mammal communication, among others.[1;2] A distinguishing feature of the oceanic medium is its heterogeneity. Plankton patches, schools of fish, marine mammals, and bubble clouds are only a few of the elements that can be found in the sea, which affect or may be affected by acoustic signals.

Bubbles in the water column are generated by several processes, such as breaking waves, cavitation from ship propellers, or even the biological action of microorganisms. Another cause of "bubbles" might be the presence of swimbladder-bearing fish. A swim bladder is an internal gas-filled organ that allows the fish to control its buoyancy and to stay at its current water depth without using energy in swimming. Acoustically, a swim bladder behaves like a damped gas bubble, and therefore the presence of large dense schools of fish can have an effect on the propagation of sound similar to that of bubble clouds. It is now known that resonant

back scattering by swim bladder-bearing fish is the major cause of volume reverberation in the ocean at frequencies up to at least 10 kHz.[3;4;5] The collective acoustic behavior of multiple gas bubbles in water continues to be a topic of great interest. In seawater, the presence of dense clouds of air bubbles can have a strong effect on the passage of sound, which impacts propagation, attenuation, scattering, and reverberation phenomena.

Over the past decades, theories of multiple scattering from bubbles in water have predominantly used time-independent descriptions. A classic approach is to consider the bubble cloud as a single scattering object, whose internal acoustic properties are described using a modified propagation wavenumber. The acoustic field due to a wave propagating through this medium can be determined by solving the corresponding Helmholtz equation. This is known as the "effective medium" model, and is based on the theory of multiple scattering of waves developed by Foldy and Carstensen.[6;7] Later on, an important study by Commander and Prosperetti[8] showed that the effective medium model underestimates the scattering amplitude in the vicinity of the resonance frequency of the bubbles, especially in dense clusters of bubbles. This can be explained by the fact that the model does not correctly represent the phenomena of acoustic interaction among bubbles, and several corrections have been subsequently proposed in order to include this effect.[9;10;11;12] Another approach to multiple scattering from bubbles is to solve a coupled differential equation system.[13] At sufficiently small amplitudes the behavior of an air-bubble in a liquid can be approximated as a simple

harmonic oscillator, represented by a mass-spring differential equation. This method incorporates both multiple scattering effects between bubbles, and coherent interactions of their individual scattered fields.[14]

In time domain modeling, the acoustic interaction between bubbles has classically been considered as an instantaneous problem.[15;16;17] For a compressible liquid, with a finite speed of sound propagation, the acoustic response of any bubble to the incident field, and to the field scattered by all the other bubbles, is a time-retarded response. Time delays directly affect the constructive or destructive interference of all the scattered fields, and therefore can be a factor of critical importance in the acoustic behavior of bubble clouds. During recent years, substantial progress has been achieved in the development of time-delay acoustic coupling in multibubble systems. The radiation forces between gas bubbles, which are also known as secondary Bjerknes forces, have been investigated for two coupled oscillating bubbles in a compressible medium,[18;19;20] as well as the forced oscillations caused by an external acoustic field.[21;22] More recent works have analyzed the time delay effects on the free oscillation of a linear bubble chain system.[23;24]

In the present work, we introduce a new method to find the impulse response of a bubble cloud in a compressible medium, based on perturbation theory.[25] This method provides for an approximate solution to the problem, by starting from the exact solution of a related linear uncoupled equation. The solution is formulated by adding interaction terms (or per-

turbations) to the mathematical description of the exactly solvable problem, incorporating the acoustic effects of the other bubbles.

The paper is organized as follows: Section II of this paper presents a general review of time domain solutions to the bubble scattering problem. Section III briefly reviews the theory and scattering models used in the proposed solution. Section IV describes the experiment that was conducted to test the model, and also describes how the data is analyzed. Section V presents the model implementation and comparison to the experimental data. A second comparison with a numerical benchmark calculation is also offered. This is followed by a summary of conclusions from our work.

# II    Review of time domain models

## II.A    Single bubble

At sufficiently small amplitudes the oscillating behavior of an air-bubble in a liquid can be approximated as a simple harmonic oscillator, represented by a mass-spring differential equation.[26;27] In his 1994 book *The Acoustical Bubble*, Leighton describes the different reference frames for the equation of motion.[15] In general, the displacement can be defined in terms of the bubble volume $\nu$ or the radius displacement $r$, while the driving term is expressed by either a force $F$ or an acoustic pressure $P$. This leads to four different combinations that

can be listed as follows:

The Radius-Pressure frame

$$m_{RP}\ddot{r}_i(t) + b_{RP}\dot{r}_i(t) + \kappa_{RP}r_i(t) = P(t), \tag{1}$$

the Volume-Pressure frame

$$m_{VP}\ddot{\nu}_i(t) + b_{VP}\dot{\nu}_i(t) + \kappa_{VP}\nu_i(t) = P(t), \tag{2}$$

the Radius-Force frame

$$m_{RF}\ddot{r}_i(t) + b_{RF}\dot{r}_i(t) + \kappa_{RF}r_i(t) = F(t), \tag{3}$$

and the Volume-Force frame

$$m_{VF}\ddot{\nu}_i(t) + b_{VF}\dot{\nu}_i(t) + \kappa_{VF}\nu_i(t) = F(t), \tag{4}$$

where the subscripts $R$, $V$, $P$, $F$ refer to "Radius," "Volume," "Pressure" and "Force," respectively. Despite the different subscripts $m$, $b$ and $\kappa$ represent the same physical concepts of mass, damping and stiffness in different frames. The exact values of these parameters will depend on the way the system is defined.

## II.B  Two bubbles

Mettin *et al.* investigated the effect of the secondary Bjerknes force in small cavitation bubbles,[17] starting from linear analysis of the equations of motion. A modified Keller-Miksis

model was used to describe the radial motion $R_i(t)$ of two spherical bubbles coupled by a time delayed term.[20] The delay $\tau$ is assumed to be equal for both mutual interactions and independent of time, which implies that the bubble radii are much smaller than the bubble separation distance $L$, and that the bubbles do not move significantly during the oscillation. Linearizing around equilibrium radii $R_i(t) = R_{i0} + r_i(t)$, the radial motion equation defined in a Radius-Pressure frame, is given by:

$$\ddot{r}_i(t) + \omega_{i0}^2 r_i(t) + f_i \dot{r}_i(t) + \frac{R_{j0}^2}{LR_{i0}} \ddot{r}_j(t - \tau) = -\frac{p_a(t)}{\rho R_{i0}}, \tag{5}$$

where $\rho$ is the water density, $f_i$ and $\omega_{i0}$ represent the damping and resonance frequency of the $i$-th bubble, and $p_a$ is the driving pressure for both bubbles. Eq. (5) assumes small amplitudes of the external sound field, i.e. $p_a << p_{amb}$, where $p_{amb}$ is the ambient pressure. Using the harmonic approach $r_i(t) = A_i e^{i\omega t}$ and $p_a = P_a e^{i\omega t}$, leads to the solution of a linear system. It should be noted that even when Eq. (5) is originally defined in the time domain, the proposed solution is time independent.

A different approach was presented by Feuillade, where the coupling effect between the bubbles is included in the mass and damping terms.[21] This work was addressed in a Volume-Pressure frame, hence it is expected that the equations differs from Eq. (5). Considering two identical bubbles pulsating in phase, the equations are:

$$m\ddot{\nu}_1 + b\dot{\nu}_1 + \kappa\nu_1 = -\delta(t) - \frac{\rho e^{-ikd}}{4\pi d}\ddot{\nu}_2,$$

$$m\ddot{\nu}_2 + b\dot{\nu}_2 + \kappa\nu_2 = -\delta(t) - \frac{\rho e^{-ikd}}{4\pi d}\ddot{\nu}_1, \tag{6}$$

where $\delta(t)$ represents the Dirac delta function, $k$ is the wavenumber, and $d$ is the distance between the bubbles. Let us asume that the damping $b$ and the coupling term $\frac{\rho e^{-ikd}}{4\pi d}$ are frequency independent, so we can perform a Fourier transform on both sides of Eqs. (6):

$$\left(-\omega^2 m + ib\omega + \kappa\right)\nu_1(\omega) = -1 + \omega^2 \frac{\rho e^{-ikd}}{4\pi d}\nu_2(\omega),$$

$$\left(-\omega^2 m + ib\omega + \kappa\right)\nu_2(\omega) = -1 + \omega^2 \frac{\rho e^{-ikd}}{4\pi d}\nu_1(\omega), \tag{7}$$

where $\omega$ is the angular frequency. Solution of equations (7) yields $\nu_1(\omega) = \nu_2(\omega) = \nu(\omega)$, then:

$$\nu(\omega) = \frac{-1}{\left(-\omega^2 m + ib\omega + \kappa - \omega^2 \frac{\rho e^{-ikd}}{4\pi d}\right)}. \tag{8}$$

Using Euler's identity in the coupling factor (i.e., $\frac{\rho e^{-ikd}}{4\pi d}$), the damping and mass terms can be re-expressed as : $m_+ = m + \frac{\rho\cos kd}{4\pi d}$, $b_+ = b + \frac{\omega\rho\sin kd}{4\pi d}$. According to Feuillade,[21] both the coupling factor and the damping deviate little over the central peak of the bubble resonance spectrum, and may be assumed practically frequency independent. Therefore, replacing

$\omega = \omega_0$ in $b_+$, $m_+$ and $k$, expression (8) yields:

$$\nu_+(\omega) = \frac{-1}{(-\omega^2 m_+ + i\omega b_+ + \kappa)}. \tag{9}$$

Performing the inverse Fourier transform of (9):

$$\nu_+(t) = -\frac{e^{-\alpha_+ t}}{m_+ \Omega_+} \sin \Omega_+ t. \tag{10}$$

Therefore, $\nu_+(t)$ represents the impulse response of the coupled system, where $\alpha_+ = \frac{b_+}{2m_+}$,

$\Omega_+ = \sqrt{\omega_{0+}^2 - \alpha_+^2}$ and $\omega_{0+} = \frac{\omega_0}{\sqrt{1 + \frac{a}{d} \cos \frac{\omega_{0+} d}{c}}}$.

## II.C   Bubble cloud

Classically, the small-amplitude free radial oscillation of $N$ coupled bubbles in a compressible

medium is described by the following equations:[15]

$$\ddot{r}_i(t) + \omega_0 \delta \dot{r}_i(t) + \omega_0^2 r_i(t) = - \sum_{m=1, m \neq n}^{N} \frac{R_{j0}}{d_{nm}} \ddot{r}_j(t - d_{nm}/c), \tag{11}$$

where $c$ is the sound speed in the water, $d_{nm}$ indicates the distance between the $n$-th and

$m$-th bubbles, and $\omega_0 \delta$ now represents the damping term. It should be noted that Eq. (11)

is essentially the same as Eq. (5) under the assumption $R_{j0} \approx R_{i0}$, for an $N$-bubble system.

In 2004, Doinikov *et al.*[23] proposed the following approximation for the time delay:

$$\ddot{r}_j(t - \tau) = \ddot{r}_j(t) - \tau \dddot{r}_j(t). \tag{12}$$

Introducing this approximation would increase the order of Eq. (11). However, it is desirable

to maintain the order of the original equation, reducing the order of Eq. (12). Let us note

that the amplitude of the coupling term is negligible in comparison to the natural radiation.

It is possible therefore to approximate Eq. (11) as:

$$\ddot{r}_i(t) \approx -\omega_0 \delta \dot{r}_i(t) - \omega_0^2 r_i(t). \tag{13}$$

Differentiating Eq. (13) and substituting into Eq. (12):

$$\ddot{r}_j(t - \tau) = (1 - \tau \omega_0 \delta) \, \ddot{r}_j(t) - \tau \omega_0^2 \dot{r}_i(t). \tag{14}$$

Substituting Eq. (14) into Eq. (11) leads to a non-delayed system. However, the approxima-

tion described in Eq. (12) may not be accurate enough for larger values of $\tau$. According to

Ref. [23], it would be valid if $\tau \ll T_0$, where $T_0 = 2\pi/\omega_0$ .

Later, Ooi and Manasseh published an extension of Doinikov's work, in which they

analyzed the time delay effects on a linear bubble chain system,[24] based on a method of

finding the eigenvalues for time delay systems developed by Hu *et al.*[28] Once the eigenvalues

$\lambda_t$ and eigenvectors $A_t$ of the time delay system are obtained, the solution in time domain can be constructed by a linear combination:

$$x(t) = \sum_{n=1}^{N} \beta_n A_{n,t} e^{\lambda_{n,t} t},$$ (15)

where $\beta_n$ are constants to be determined from the initial conditions.

# III Theory

In this section we describe briefly the perturbation theory, and its application to the solution of the impulse response of a bubble cloud, incorporating the interactions in a series of equations that add the contributions of the other bubbles.

## III.A Simple perturbation theory

Consider an equation defined by an operator $L$ such as:

$$L\phi(x) = f(x),$$ (16)

where $\phi(x)$ is any function that satisfies Eq. (16). Typically, in multiple degrees-of-freedom problems, the resulting equation (16) cannot be solved. However, let us consider the following

equation with a direct solution:

$$L_0\phi_0(x) = f(x). \tag{17}$$

Suppose that the operator $L$ can be written as follows:

$$L = L_0 + \epsilon L_I, \tag{18}$$

where $\epsilon$ is a small quantity and the subscript $I$ refers to "interaction." [25] Let us note that Eq. (16) is not the same as Eq. (17), and thus $\phi \neq \phi_0$. Now we assume that the exact solution $\phi(x)$ can be expressed as follows:

$$\phi(x) = \phi_0(x) + \epsilon\phi_1(x) + \epsilon^2\phi_2(x) + ..., \tag{19}$$

where $\phi_0$, $\phi_1$, $\phi_2$ denote the coefficients of the $\epsilon$-expansion. If $\epsilon$ is small, Eq. (19) can be truncated at a low order. Substituting from (19) and (18) in (16):

$$f(x) = L_0\phi_0(x) + L_0\epsilon\phi_1(x) + L_0\epsilon^2\phi_2(x),$$
$$+ \epsilon L_I\phi_0(x) + \epsilon^2 L_I\phi_1(x) + O(\epsilon^3), \tag{20}$$

and then equate coefficients of each power of $\epsilon$ in (20):

$$\epsilon^0 : L_0\phi_0(x) = f(x), \tag{21}$$

$$\epsilon^1 : L_0\phi_1(x) = -L_1\phi_0(x), \tag{22}$$

$$\epsilon^2 : L_0\phi_2(x) = -L_1\phi_1(x). \tag{23}$$

Now we have a set of equations for $\phi_0$, $\phi_1$, $\phi_2$, which form the solution $\phi$ in Eq. (19). The coefficients are then calculated iteratively, beginning with $\phi_0$. Once we solve (21), $\phi_0$ is used as an input of (22), and so on. In the previous derivation, $\epsilon$ is assumed to be small enough to truncate expansion (19) at a low order. Let us now define the interaction operator by:

$$L_I = L - L_0, \tag{24}$$

which is equivalent to $L = L_0 + \epsilon L_I$, where $\epsilon = 1$. In this case, we can still follow the methods of perturbation theory, as if for small $\epsilon$, and calculate the coefficients iteratively, but now there is no basis for truncating the expansion.

## III.B   Encapsulated bubbles

In a classic work published in 1989 by Commander and Prosperetti, a rigorous model for the propagation of pressure waves in bubbly liquids was formulated.[8] Combining Eqs. (27) and (32) from Ref. [8] yields to a linearized expression for the resonance frequency of the radial

motion of a non-encapsulated and isolated bubble:

$$\omega_0^2 = \frac{P_0}{\rho_l a^2} \left( 3\gamma - \frac{2\sigma}{aP_0} \right),$$

(25)

where $a$ indicates the bubble equilibrium radius, $P_0$ is the undisturbed pressure in the bubble, $\rho_l$ is the liquid density, $\sigma$ is the surface tension at the liquid-gas interface and $\gamma$ represents the ratio of specific heats in air.

Church derived a model for a collection of encapsulated bubbled, by considering an elastic shell in the liquid-air interface. Since the resonance frequency and the damping are affected by the shell, it was necessary to develop new expressions for those parameters:[29]

$$\omega_0^2 = \frac{P_0}{\alpha \rho_s a_1^2} \left\{ 3\gamma - \frac{2}{P_0} \left( \frac{\sigma_1}{a_1} + \frac{\sigma_2}{a_2} \frac{a_1^3}{a_2^3} \right) + \frac{4V_s G_s}{a_2^3 P_0} \left[ 1 + Z \left( 1 + \frac{3a_1^3}{a_2^3} \right) \right] \right\},$$

(26)

$$Z = \left[ \frac{2\sigma_1}{a_1} + \frac{2\sigma_2}{a_2} \right] \frac{a_2^3}{V_s} \frac{1}{4G_s},$$

$$\alpha = \left[ 1 + \left( \frac{\rho_l - \rho_s}{\rho_s} \right) \frac{a_1}{a_2} \right],$$

where $\rho_s$, $G_s$ represent the density and shear modules of the shell material; $a_1, a_2$ are the internal and external bubble radius, $V_s$ is defined as $a_2^3 - a_1^3$ and $\sigma_1, \sigma_2$ denote the surface tension of the gas-shell and shell-liquid interfaces, respectively.

The terms for the viscous damping in the liquid, the thermal damping, and acoustic re-radiation damping also contain modifications due to the presence of the shell:

$$\beta_{\text{vis},L} = \frac{2\mu_l}{\rho_s a_1^2} \frac{a_1^3}{a_2^3 \alpha}, \qquad \beta_{\text{th}} = \frac{2\mu_{\text{th}}}{\rho_s a_1^2 \alpha}, \qquad \beta_{\text{ac}} = \frac{\omega}{c} \left(\frac{\omega a_2}{c}\right) \left[1 + \left(\frac{\omega a_2}{c}\right)^2\right]^{-1}, \tag{27}$$

where $\mu_l$ is the liquid viscosity. An expression for the thermal viscosity $\mu_{\text{th}}$ may be found in Eq. (14) from Ref. [30]. Substitution of $\mu_{\text{th}}$ into $\beta_{\text{th}}$ yields:

$$\beta_{\text{th}} = \frac{P_0}{2\rho_s \omega a_1^2 \alpha} \text{Im}(\Phi), \tag{28}$$

where

$$\Phi = \frac{3\gamma}{1 - 3(\gamma - 1)i\chi \left[(i/\chi)^{1/2} \coth(i/\chi)^{1/2} - 1\right]}, \tag{29}$$

and $\chi = D/\omega a_1^2$ , where $D$ is the gas thermal diffusivity . The expressions of $\Phi$ and $\chi$ correspond to Eqs. (27) and (28) of Ref. [8], respectively.

The new damping term also incorporates an additional term for the viscous damping due to the shell material of viscosity $\mu_s$.

$$\beta_{\text{vis},s} = \frac{2\mu_s}{\rho_s a_1^2} \frac{V_s}{a_2^3 \alpha}. \tag{30}$$

## III.C   Time domain coupled differential equations (CDE) for a bubble cloud

In 1996, Feuillade *et al.* developed a scattering model which includes all the multiple interaction among the bubbles. If we consider an external field driving an ensemble of $N$ interacting bubbles, the total field incident on any bubble is the sum of the external field and the fields scattered from all the other bubbles. The response of a whole group may be represented by a set of coupled differential equations as follows:[14]

$$m_n\ddot{\nu}_n + b_n\dot{\nu}_n + \kappa_n\nu_n = -P_n e^{i(\omega t + \phi_n)} - \sum_{j\neq n}^{N} \frac{\rho e^{-ikr_{jn}}}{4\pi r_{jn}}\ddot{\nu}_j, \tag{31}$$

where the subscript $n$ refers to the $n$-th bubble and $\nu$ is the differential volume (i.e., the difference between the instantaneous and equilibrium bubble volumes). The coefficient $m(=\rho/4\pi a)$ is termed the inertial "mass" of the bubble, where $a$ is the bubble radius, and $\kappa(=3\gamma P_A/4\pi a^3)$ is the "adiabatic stiffness". $P_n$ and $\phi_n$ are the amplitude and phase respectively of the external field experienced by the $n$-th bubble, and $r_{jn}$ is the radial distance from the center of the $n$-th bubble to the center of the $j$-th bubble. Harmonic "steady-state" solutions of these coupled equations are found by substituting $\nu_n = \bar{\nu}e^{i\omega t}$ in Eq. (31). This leads to a matrix equation which can be solved by matrix inversion.

However, this analysis has been carried out in the frequency domain, where the time delays are represented as additional phase terms. In order to calculate the impulse response

of the bubble cloud, a time domain version of the CDE method is proposed, equivalent to

the equations of Ooi and Manasseh:[24]

$$m_i \ddot{\nu}_i + b_i \dot{\nu}_i + \kappa_i \nu_i = -\delta(t - t_i) - \sum_{\substack{i \neq j}}^{N} \frac{\rho}{4\pi r_{ij}} \ddot{\nu}_j(t - t_{ji}), \tag{32}$$

where $\delta(t - t_i)$ represents an impulse arriving at $t = t_i$ to the $i$-th bubble, and the coupling

term $\sum_{i \neq j}^{N} \frac{\rho}{4\pi r_{ij}} \ddot{\nu}_j(t - t_{ji})$ is the coherent summation of the pressure fields radiated by the

remaining $N$-1 bubbles within the cloud. Let us note that the coupling term $\ddot{\nu}_j(t - t_{ji})$

includes the time delay $t_{ji}$ between each pair of bubbles. The coupled system described in

Eq. (32) can be written in state space, such that:

$$\dot{\mathbf{x}} - \mathbf{A_0}\mathbf{x} = \mathbf{Bu} + \operatorname{diag}\left(\mathbf{A_I}\dot{\mathbf{x}_R}\right), \tag{33}$$

where

$$\mathbf{x} = \begin{bmatrix} \nu_1 \\ \vdots \\ \nu_N \\ \dot{\nu}_1 \\ \vdots \\ \dot{\nu}_N \end{bmatrix}_{2N \times 1} , \ \mathbf{A_0} = \begin{bmatrix} \mathbf{0}_{N \times N} & \mathbf{I}_{N \times N} \\ -\mathbf{M}^{-1}\mathbf{K} & -\mathbf{M}^{-1}\mathbf{C} \end{bmatrix}_{2N \times 2N} , \ \mathbf{B} = \begin{bmatrix} \mathbf{0}_{N \times N} \\ -\mathbf{M}^{-1} \end{bmatrix}_{2N \times N}$$

$$\mathbf{E} = \begin{bmatrix} 0 & \frac{\rho}{4\pi r_{12}} & \cdots & \frac{\rho}{4\pi r_{1N}} \\ \frac{\rho}{4\pi r_{21}} & \ddots & \cdots & \frac{\rho}{4\pi r_{2N}} \\ \vdots & \vdots & \ddots & \vdots \\ \frac{\rho}{4\pi r_{N1}} & \frac{\rho}{4\pi r_{N2}} & \cdots & 0 \end{bmatrix}_{N \times N} , \ \mathbf{C} = \begin{bmatrix} b_1 & 0 & \cdots & 0 \\ 0 & b_2 & \cdots & 0 \\ \vdots & \vdots & \ddots & \vdots \\ 0 & 0 & \cdots & b_N \end{bmatrix}_{N \times N} ,$$

$$\mathbf{A_I} = \begin{bmatrix} \mathbf{0}_{N \times N} & \mathbf{0}_{N \times N} \\ \mathbf{0}_{N \times N} & \mathbf{M}^{-1}\mathbf{E} \end{bmatrix}_{2N \times 2N} , \ \dot{\mathbf{x}_R} = \begin{bmatrix} \mathbf{0}_{N \times N} & \mathbf{0}_{N \times N} \\ \mathbf{0}_{N \times N} & \ddot{\nu}_R \end{bmatrix}_{2N \times 2N} ,$$

$$\mathbf{M} = \begin{bmatrix} m_1 & 0 & \cdots & 0 \\ 0 & \ddots & \cdots & 0 \\ \vdots & \vdots & \ddots & \vdots \\ 0 & 0 & \cdots & m_N \end{bmatrix}_{N \times N}, \mathbf{K} = \begin{bmatrix} \kappa_1 & 0 & \cdots & 0 \\ 0 & \kappa_2 & \cdots & 0 \\ \vdots & \vdots & \ddots & \vdots \\ 0 & 0 & \cdots & \kappa_N \end{bmatrix}_{N \times N},$$

$$\mathbf{u} = \begin{bmatrix} \delta(t - t_1) \\ \delta(t - t_2) \\ \vdots \\ \delta(t - t_N) \end{bmatrix}_{N \times 1} \text{ and } \ddot{\nu}_R = \begin{bmatrix} 0 & \ddot{\nu}_1(t - t_{12}) & \cdots & \ddot{\nu}_1(t - t_{1N}) \\ \ddot{\nu}_2(t - t_{21}) & \ddots & \cdots & \ddot{\nu}_2(t - t_{2N}) \\ \vdots & \vdots & \ddots & \vdots \\ \ddot{\nu}_N(t - t_{N1}) & \ddot{\nu}_N(t - t_{N2}) & \cdots & 0 \end{bmatrix}_{N \times N}$$

If we leave the term $\text{diag}\left(\mathbf{A_{I}}_{2N \times 2N}\dot{\mathbf{x}}_{\mathbf{R}2N \times 2N}\right)$ out of Eq. (33), the remaining equation

takes the form of a linear system with input $\mathbf{u}(t)$, which can be solved by conventional

methods.[31;32] Considering the term $\text{diag}\left(\mathbf{A_{I}}_{2N \times 2N}\dot{\mathbf{x}}_{\mathbf{R}2N \times 2N}\right)$ as an external perturbation,

the methodology described in Section III.A can be used to obtain the solution of Eq. (33):

$$L(\mathbf{x}) = \mathbf{Bu}, \tag{34}$$

where

$$L = L_0 + \epsilon L_I,$$

$$L_0 : \frac{d}{dt} - \mathbf{A_0}, \tag{35}$$

$$L_I : -\mathbf{A_I}\frac{d}{dt}.$$

If $\epsilon = 1$ , the operator $L$ leads to the exact solution of Eq. (33). Following the methodology

described in Section III.A (Eqs. 19 to 23), the problem is re-expressed as:

$$\epsilon^0 : L_0\phi_0 = f \longrightarrow \dot{\phi}_\mathbf{0} - \mathbf{A_0}\phi_\mathbf{0} = \mathbf{Bu}, \tag{36}$$

$$\epsilon^1 : L_0\phi_1 = -L_1\phi_0 \longrightarrow \dot{\phi}_\mathbf{1} - \mathbf{A_0}\phi_\mathbf{1} = -\mathbf{A_I}\dot{\phi}_\mathbf{0}, \tag{37}$$

$$\epsilon^2 : L_0\phi_2 = -L_1\phi_1 \longrightarrow \dot{\phi}_\mathbf{2} - \mathbf{A_0}\phi_\mathbf{2} = -\mathbf{A_I}\dot{\phi}_\mathbf{1}. \tag{38}$$

## III.D    Solving the uncoupled problem

Since the input $\mathbf{u}$ of the uncoupled problem $\dot{\phi}_\mathbf{0} - \mathbf{A_0}\phi_\mathbf{0} = \mathbf{Bu}$ consists of a series of impulses,

an analytic solution can be found for $\phi_\mathbf{0}$. Since the arrival time depends upon the distance

between the source and each bubble, a solution of the type $\mathbf{RI} = e^{\mathbf{A}t}\mathbf{B}\begin{bmatrix} 1 & 1 & 1\dots 1 \end{bmatrix}^T$ cannot

be applied in this case. It is possible to derive a concise analytic solution using a matrix

exponential, however the computational cost would be considerable for bigger clouds. The

computational cost will depend on the number of discrete time steps, and the size of matrix

**A₀**. For example, if $N = 500$, and if a time step of 0.1 ms is used, solving for a 1s time segment of $\phi_0$ would take approximately 3 hours using the direct matrix exponential approach, and less than one minute using a modal solution (simulations were performed on a 1.6 GHz Intel Core i5 processor). On the other hand, the largest size matrix that can be handled ($N \sim$ 10,000) will depend on the available system memory and the operating system. Therefore, a modal coordinates solution is proposed:

$$\sigma_j(t) = \int_0^t e^{\lambda_j(t-\tau)} \widetilde{\mathbf{B}}(j,:)\mathbf{u}(\tau)d\tau, \tag{39}$$

$$\phi_0 = \mathbf{\Psi}\sigma \qquad \sigma : \text{new coordinates}, \tag{40}$$

where $\lambda_i$ are the eigenvalues of $\mathbf{A_0}$, $\mathbf{\Psi}$ is the matrix whose columns are the eigenvectors of $\mathbf{A_0}$. $\widetilde{\mathbf{B}}(j,:)$ corresponds to the $j$-th column of the product $\mathbf{\Psi}^{-1}\mathbf{B}$. Let us note that the product $\widetilde{\mathbf{B}}(j,:)\mathbf{u}$ is a scalar quantity. Assuming zero initial conditions for all the variables, Eq. (39) may be re-expressed as:

$$\sigma_j(t) = \int_0^t e^{\lambda_j(t-\tau)}[\widetilde{\mathbf{B}}(j,1)\delta(\tau - t_1) + \ldots + \widetilde{\mathbf{B}}(j,N)\delta(\tau - t_N)]d\tau.$$

Using Dirac delta properties:

$$\sigma_j(t) = e^{\lambda_j(t-t_1)}\widetilde{\mathbf{B}}(j,1) + \ldots + e^{\lambda_j(t-t_N)}\widetilde{\mathbf{B}}(j,N). \tag{41}$$

# IV  Data analysis

A series of experiments were performed at the Lake Travis Test Station, Applied Research Laboratories (ARL, The University of Texas at Austin), to measure the attenuation of sound through an artificial bubble cloud, consisting of 14 fixed air-filled latex balloons of 4.68 cm radius at the surface.[33;34] The balloons were attached by a nylon netting grid to a steel cage of dimensions 1.22 m wide by 1.30 m deep by 1.30 m tall, as shown in Figure 1. Three balloon configurations were used, but in the present work just one of them was analyzed.

The source was a Navy J-13, which is an approximately omnidirectional electromagnetic loudspeaker designed to operate between 30 and 3000 Hz at depths up to 20 meters. Linear chirps from 30 Hz to 2 kHz produced by the J-13 were recorded by nine HTI-90-U hydrophones, located at 2 meter intervals of depth from 2 meters to 18 meters, at a horizontal distance of 11.7 meters from the center of the bubble cloud, as shown in Figure 2.

The source signal and all the hydrophone signals were digitized by a Data Translation DT9837B data acquisition module. Transfer functions between each hydrophone signal and the source signal were calculated using Data Translation's VIBPoint Framework software. These transfer functions represent the acoustic pressure recorded at each hydrophone normalized by the source signal voltage. Transfer functions were measured with and without the bubble cloud. A measurement technique that had been previously used to study small
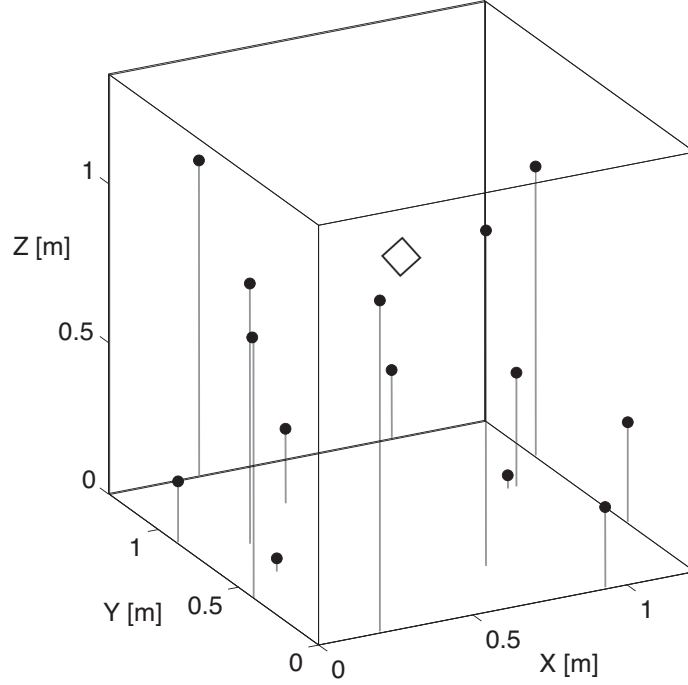
Figure 1: The location of each of the 14 balloons is shown along with a local coordinate system associated with the steel frame that held the balloons. The balloon locations appear in Table G.3 of Ref. [33]. The source is depicted with the diamond-shape symbol.

bubbles was used here to isolate the acoustic effect of the bubble cloud scattering.[35] According to this technique, the received signal at the measurement hydrophone $y(t)$, can be considered as the superposition of two components, i.e.,
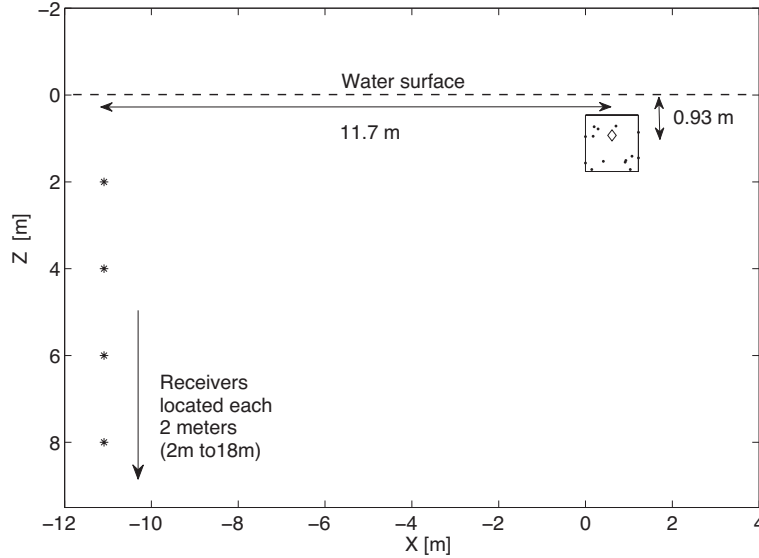
$$y(t) = y_d(t) + y_s(t), \tag{42}$$

Figure 2: Experimental apparatus. The water depth at the source position was 19.6 m and the depth at the receiver position was 19.1 m. The bubble frame and the source are shown on the right. The source is depicted by the diamond symbol. The air-filled balloons are depicted by the solid black dots. On the left, the hydrophones are depicted using asterisks. The source was located at a depth of 0.93 m from the surface.

where $y_d(t)$ is the signal due to the direct field (in the absence of bubbles), and $y_s(t)$ is the signal arising from the acoustic field generated by scattering from the bubble cloud. It is possible then to estimate the field scattered from the bubbles by subtracting the two measurable quantities $y_d(t)$ and $y_s(t)$. The difference between those quantities shows the impact of adding bubbles to the system.

Transfer functions are generally defined in the frequency domain, and represented as a complex function of the frequency. The corresponding impulse response (i.e. the time domain representation of the transfer function) can be obtained by performing an inverse Fourier transform (IFFT). Since the Fourier transform is a linear operator, the superposition defined in Eq. (42) is valid in both the frequency and time domains. After the subtraction, nine different curves were found, corresponding to the nine hydrophone locations. Each curve represents the transfer function for the bubble group, measured at a given depth.

According to the classic wave theory, the phase relation between the driving oscillation and the oscillation of the bubble depends upon the frequency: they are in phase with each other below resonance, they are in quadrature at resonance, and in anti-phase above resonance.[36] Figure 3 shows the phase as a function of frequency, for the measured transfer function (solid line). The dash-dot line represent the predicted phase response of the bubble group, calculated with a frequency dependent model developed by Feuillade *et al.* in 1996.[14] Both the modeled and measured phase response show the reversal of phase for frequencies above the resonance.

It has been reported in the literature that shallow water measurements exhibit a strongly nonlinear phase, especially at low frequency. This behavior suggests that the sub-bottom structure plays an important role in sound reflection. By contrast, a linear cross-spectral phase would imply that the source-receiver propagation is dominated by a single path.[37]
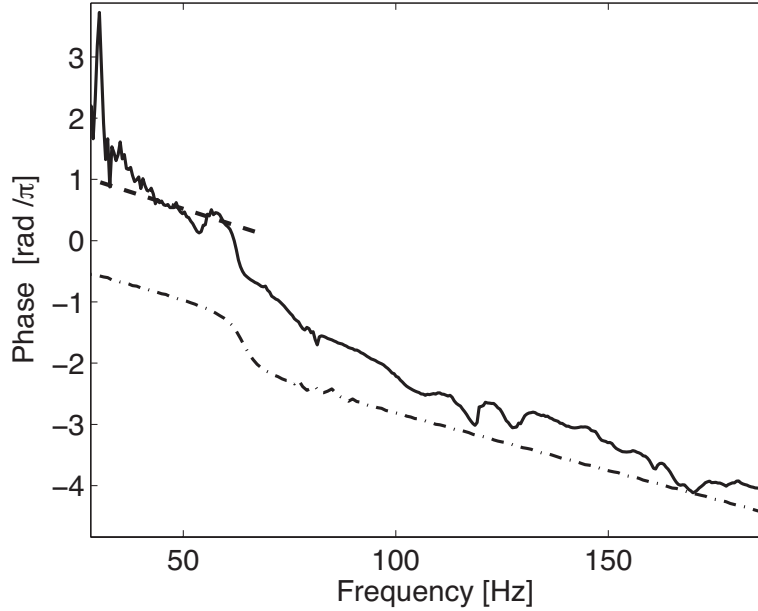
Figure 3: Phase response of the bubble cloud for the receiver located at 6 m depth. Solid line: phase of the measured transfer function, after the subtraction. Dash-dot line: theoretical phase response, calculated using a frequency dependent scattering model.[14] The dashed line represents the slope of the measured phase in the linear zone below resonance. For the phase adjustment, the measured curve was transposed until the dashed line coincided with the dash-dot line. In other words, the measured phase was adjusted to match the predicted phase below the resonance frequency.

Measurements performed in Lake Travis also exhibit the nonlinear phase behavior (solid line in Figure 3), which confound the comparison with theoretical predictions. Since scattering

models are usually developed in the free field and subsequently included as an input in full propagation models, it is not intended to incorporate reflections from layered boundaries in the present work. A phase adjustment of the measured data was performed, which is depicted in Figure 3.

# V    Results

## V.A    Model Implementation

A time-domain model was implemented to calculate the impulse response of a cloud of bubbles, based on the perturbation theory solution explained in Section III.C. The model was tested against the transfer functions measured in Lake Travis for the group of fixed balloons. This technique was also compared with a numerical benchmark, which includes all the multiple interactions and time delays.

It is first necessary to determine a number of input parameters, to provide a starting point to run the bubble scattering model. The model requires information about the bubble size, damping, and individual resonance frequency. It is also required to know the relative positions among the source, bubbles and receiver, which strongly affect the individual phase response, and therefore, the total interference pattern. In the present experiment, all the relative positions of the balloons are known, as well as their individual radii at the water surface. For each balloon, the radius during deployment is corrected for hydrostatic pressure

at the corresponding depth.

**Table I: Input parameters to the encapsulated bubble model.**

| Parameter | Symbol | Value | Units |
|---|---|---|---|
| Shell material density | $\rho_s$ | 933 [a] | kg/m$^3$ |
| Shear modulus of shell | $G_s$ | 0.75 [b] | MPa |
| Liquid density | $\rho_l$ | 998 | kg/m$^3$ |
| Liquid viscosity | $\mu_l$ | 0.001 | MPa |
| Internal radius | $a_1$ | 4.68 | cm |
| Shell wall thickness | $r_s$ | 0.254 | mm |
| Ratio of specific heats (air) | $\gamma$ | 1.4 | |
| Thermal conductivity for air | $D$ | $2 \times 10^{-5}$ | m$^2$/s |
| Surface tension in gas-shell interface | $\sigma_1$ | 25 [c] | N/m |
| Surface tension in shell-liquid interface | $\sigma_2$ | 5 | N/m |
| Hydrostatic pressure at mean bubble depth | $P_0$ | $1.12 \times 10^5$ | Pa |

[a] Measured for the specific shell material used in the experiment (unpublished).

[b] Mean value over the range 10-2000 Hz.

[c] Following Lee *et al.*,[38] $\sigma_1$ and $\sigma_2$ were selected such that their sum was equal to 30. The value of each tension is less important that the sum of both, due to the very small difference between the internal and external radii.

The physical parameters input to the modified resonance frequency model and damping given by Eqs. (26) to (30) are summarized in Table I. The shear modulus and viscosity were not measured for the specific shell material used in the experiment. Following Lee *et al.*,[38] these parameters were estimated using viscoelastic master curves that were obtained for natural rubber. In this work, an AA 165-5 formulation for natural rubber was used. The coefficients for generating these master curves were extracted from p. 147 of Ref. [39], and are summarized on Table II.

**Table II: Master curves for AA 165-5**

| Coefficient | Young storage modulus ($E'$) | Loss factor ($\tan \delta$) |
|:-----------:|:----------------------------:|:---------------------------:|
| $c_0$ | 6.1183 | -0.81459 |
| $c_1$ | -0.07094 | -0.54046 |
| $c_2$ | 0.11964 | 0.35967 |
| $c_3$ | -0.043413 | -0.044629 |
| $c_4$ | 0.0067797 | – |

$$\log_{10}(E' \text{ or } \tan \delta) = \sum c_n [\log_{10} \text{freq.(Hz)}]^n$$

Figure 4 shows the damping components calculated for the 10 Hz to 2000 Hz frequency range. The total damping was calculated as $\beta_{\text{total}} = \beta_{\text{ac}} + \beta_{\text{th}} + \beta_{\text{vis},L} + \beta_{\text{vis},s}$. Since the IR model implemented is a time-domain method, a frequency dependent damping parameter
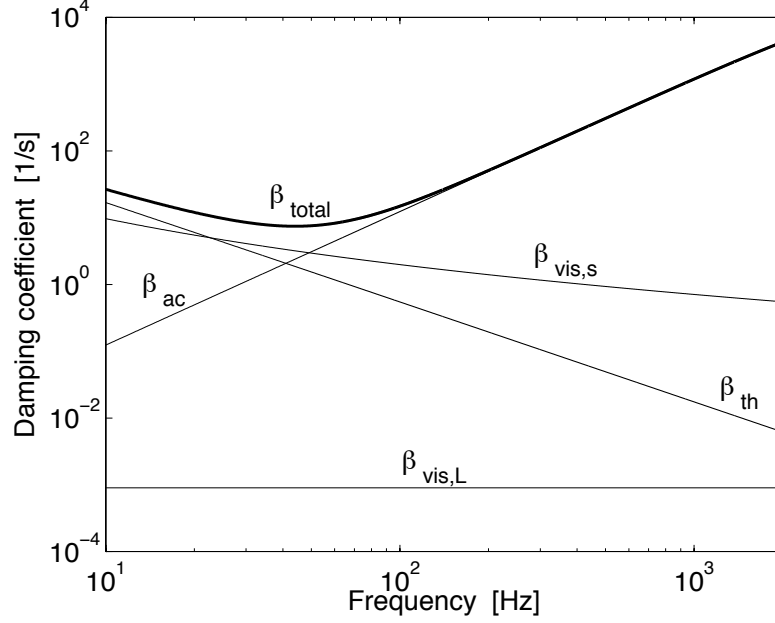
Figure 4: Dimensional linear damping constants versus frequency for a bubble radius of 4.68 cm. The components $\beta_{ac}, \beta_{th}, \beta_{vis,L}, \beta_{vis,s}$ were calculated using the expressions given by Eqs. (26) to (30) and the physical parameters indicated in Table I. An AA 165-5 formulation for natural rubber was used. The coefficients for generating these master curves are given on p. 147 of Ref. [39].

cannot be included. Therefore, a constant value was used in the model implementation, corresponding to the total damping at the resonance frequency $\beta_{\text{total}} \approx 10$. Future work should include a time dependent damping parameter, which responds in a different way to transient and stationary states.

The individual bubble resonance frequency is also affected by the elastic shell. Using Church's model from Eq. (26) with the physical parameters indicated in Table I, a resonance frequency of 77 Hz was predicted for the bubble size used in the present experiment. However, a discrepancy between measurements and the Church model prediction has recently been reported. According to Lee *et al.*,[38] for balloon radii ranging from 1.6 cm to 3.5 cm, the measured resonance frequencies of the natural latex balloons deviated from Church's model by 11% or less. Subsequent adjustments indicate a better match for a resonance frequency of 83 Hz, which is similar to the deviation reported by Lee *et al.*,[38] under similar circumstances.

Once the Eqs. (32) are solved, the total scattered pressure field for the whole group is given by the coherent summation:[40]

$$p_s(r) = \frac{\rho_l}{4\pi r} \sum_{i=1}^{N} \ddot{v}_i(t - t_{ri}), \tag{43}$$

where $\rho_l$ is the liquid density, and $t_{ri}$ is the time delay between the receiver and the $i$-th bubble. The scattered pressure field $p_s(r)$ represents the impulse response of the bubble group in the free field, i.e. in the absence of boundary reflections.

## V.B   Perturbation Theory Solution

The inputs previously determined were used to formulate the operators $L_0$ and $L_I$, defined in Eq. (35). As it was previously formulated, the solution of the coupled system (32) is defined as the expansion in $\epsilon$: $\phi(t) = \phi_0(t) + \epsilon\phi_1(t) + \epsilon^2\phi_2(t) + ....$ The first term of the expansion

corresponds to the solution of equation (36), which can be analytically solved using expression (41). The functions $\phi_n$ were iteratively calculated as the solution of $\dot{\phi}_\mathbf{n} - \mathbf{A_0}\phi_\mathbf{n} = -\mathbf{A_I}\dot{\phi}_{n-1}$, using a fourth order Runge-Kutta algorithm. According to Eq. (35), a value of $\epsilon = 1$ was used in this work.

According to Ref. [25], even when $\epsilon$ is small, the perturbation expansion is not convergent. However, in practice one may still obtain a good approximation to $\phi(t)$ by taking a finite number of terms and neglecting the remainder (asymptotic convergence). In order to truncate the expansion, a criterion must be introduced. Let us say that convergence is reached when the relative error between $\phi_n$ and $\phi_{n+1}$ is less than a tolerance value. The convergence of the $\epsilon$-expansion will be determined by the interaction operator $L_I$. In our case, $L_I$ depends upon the matrix $A_I$, which consist of all the acoustic interactions between bubbles. Since all $\phi_n$ functions are related to $\phi_0$, the operator $L_I$ will also depend upon the physical parameters included in $A_0$. Figure 5 shows the number $N$ of terms required for convergence, for selected values of individual resonance frequency and distance among the scatters. Since $\phi_N$ incorporates the differential volume and its first derivative for all the fourteen bubbles, the convergence analysis was performed just over one bubble, i.e., the first element of $\phi_N$. A tolerance value of $10^{-6}$ was used as a convergence criterion. The simulated time was 0.3 seconds, with a time step of $10^{-4}$ seconds.

As the operators $L_I$ and $L_0$ are defined for this case, the amplitude for $\phi_n$ grows expo-
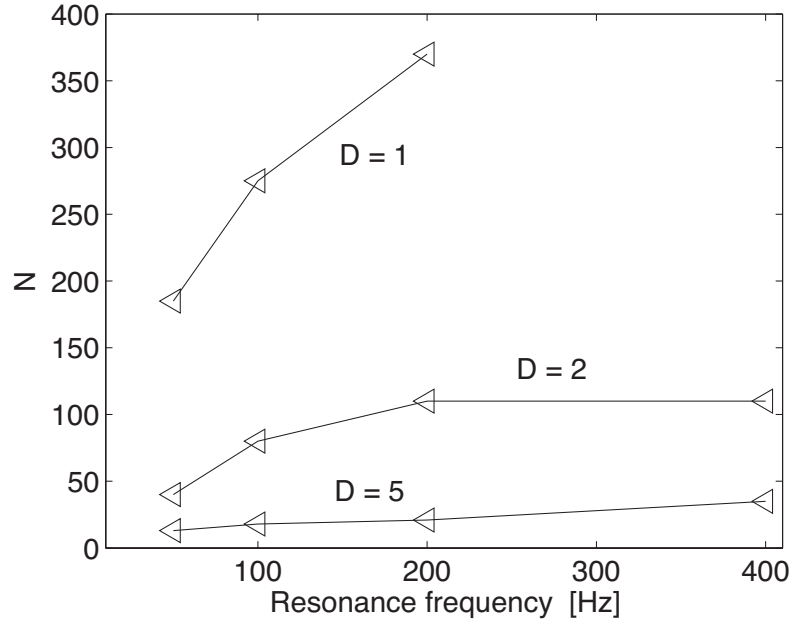
Figure 5: Simulations were performed for individual resonance frequencies of 50 Hz, 100 Hz, 200 Hz and 400 Hz, at the actual distances between the fourteen bubbles (D=1), and modifying the inter-bubble distance by a factor of two (D=2) and five (D=5). $N$ is the number of terms for which the expansion converges in each case ($\triangleleft$). Different resonance frequencies may correspond to different bubble sizes or depths, and are included in $A_0$. The distance between the scatterers are incorporated in the interaction matrix $A_I$.

nentially with $n$. For higher orders of $n$ the solutions will require extended precision, which would imply significantly higher computational cost. Therefore, an alternative methodology was implemented, based on the decay of the impulse response. It can be noticed from Figure

6, that higher orders of $\phi_n$ affect later times. In other words, a longer simulation window will require more functions $\phi_n$ to converge to the solution $\phi$. Since the amplitude of $\phi$ decays with time, the later time points will not depend strongly on the first ones. Therefore, it is possible to stop the computations at a certain time $t = \tau$, and restart it again as an initial value problem for the next time window. In this way, all the $\phi_n$ functions will be calculated up to $t = \tau$, and added together to obtain the solution $\phi$. For the next time window, a new $\phi_0$ is obtained as the solution of the initial value problem $\dot{\phi}_\mathbf{0} - \mathbf{A_0}\phi_\mathbf{0} = 0$, where the initial condition $\phi_0(\tau)$ corresponds to $\phi(t = \tau)$, i.e. the last value of the solution $\phi$ for the first window. For the second time window, all the $\phi_n$ functions must be calculated using the new $\phi_0$. The simulation can be rebooted as many times as needed. In this way, a long time window can be split into shorter windows of length $\tau$, reducing the order of the $\phi_n$ functions needed, and therefore, the computing time.

However, the solution cannot be restarted time to time, since the input term in $\dot{\phi}_\mathbf{n} - \mathbf{A_0}\phi_\mathbf{n} = -\mathbf{A_I}\dot{\phi}_{n-1}$ consists of past values of $\phi_{n-1}$. Consequently, each reboot will lose some information about the first time steps, when no past values are available. Accordingly, the time interval $\tau$ should be long enough so that the missing values are negligible compared to the interval. The value of $\tau$ can be chosen as the mean lifetime of $\phi_0$, i.e. $\tau = \frac{1}{\lambda}$, where $\lambda$ denotes the average eigenvalue of $A_0$. Since the interaction between bubbles adds damping to the system, the decay of $\phi_0$ will be the minimum decay of the total system.
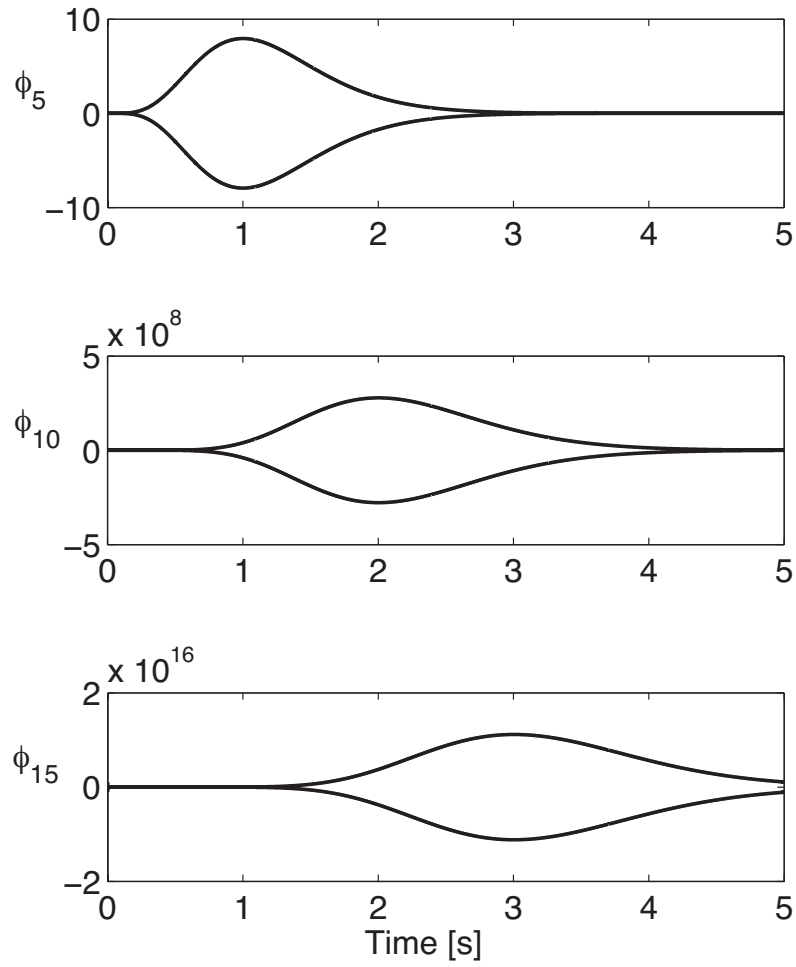
Figure 6: (a) $\phi_5$ , (b) $\phi_{10}$ , (c) $\phi_{15}$. Only the envelope of the functions are shown in the figure. Note the variation of the maximum amplitude in each case.

## V.C  Perturbation - Benchmark comparison.

A numerical benchmark was also implemented to solve Eqs. (32), using a fourth order Runge-Kutta algorithm. Looking at Eq. (33), the input consists of two terms: the impulse signal coming from the source ($\mathbf{Bu}$) and the multiple scattering among the bubbles ($\mathbf{A_I \dot{x}_R}$). The input $\mathbf{u}$ consists of a series of delayed impulses $\delta(t-t_n)$, where the arrival time $t_n$ will depend upon the distance between the source and the $n$-th bubble. Since both the impulse and the acoustic interactions are delayed, for each time step the input will depend on past values of $\mathbf{x}$, which were already calculated. For the first time steps, there will be some cases when the interaction delays lead to negative values. This implies that the scattered field from one bubble has not yet reached the other bubbles. In which cases, there is no interaction between the two bubbles and the corresponding term is zero.

An additional difficulty is the impulse implementation. The Dirac delta function can be numerically represented as the limit of a Gaussian function, such as[41]

$$\delta(x - x') = \lim_{\xi \to 0} \frac{1}{\sqrt{\xi \pi}} e^{-\frac{(x-x')^2}{\xi}}. \tag{44}$$

In the limit $\xi \to 0$, the amplitude of this function goes to infinity, while its width goes to

zero. For any $\xi \neq 0$,

$$\int_{-\infty}^{\infty} \frac{1}{\sqrt{\xi \pi}} e^{-\frac{(x-x')^2}{\xi}} \, dx = 1. \tag{45}$$

This relation holds for any $\xi$. For the input implementation, the value of $\xi$ was calibrated by matching the general amplitude and shape of the numerical benchmark and the perturbation-based solution. Figure 7(a) shows the impulse response for the differential volume of one bubble, when $\xi = 0.0077$. A reasonable agreement between the numerical benchmark and the perturbation-based solution is observed from Figure 7(a). The similarity of two signals $X$ and $Y$ can also be determined using a mathematical tool called magnitude squared coherence (MSC). The coherence spectrum is defined by the squared cross spectrum divided by the product of the two autospectra:[42]

$$C_{XY}(\omega) = \frac{|G_{XY}(\omega)|^2}{G_{XX}(\omega) \cdot G_{YY}(\omega)}, \tag{46}$$

where $\omega$ indicates the frequency domain, $G_{XY}$ is the cross spectral density, and $G_{XX}, G_{YY}$ are the autospectra of signals $X$ and $Y$, respectively. Figure 7(b) shows the MSC estimator when $X$ denotes the perturbation-based solution and $Y$ is the numerical benchmark. The MSC was calculated using Welch's overlapped averaged periodogram method,[43] which is implemented in the MATLAB Signal Processing Toolbox (*mscohere*). The coherence is nearly always very close to unity, except for a region around the individual bubble resonance, where it has a
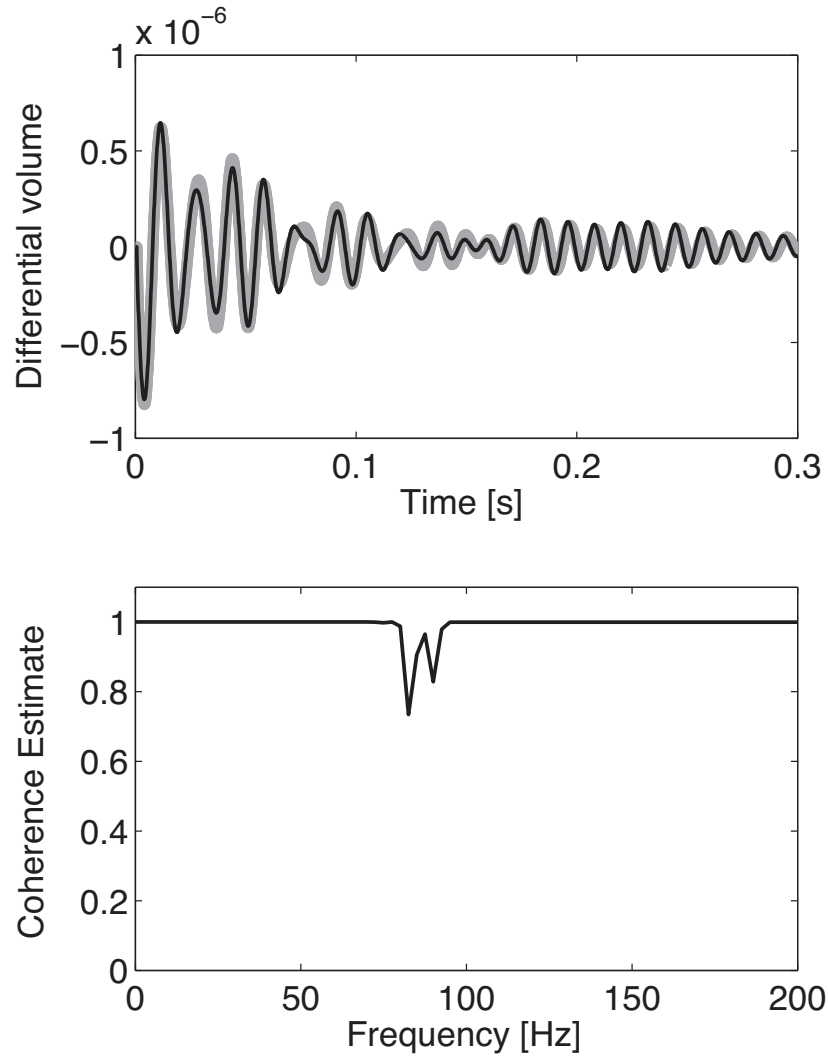
Figure 7: (a) Theoretical comparison between numerical benchmark (gray line) and the perturbation-based solution (black line). (b) Coherence estimator between both curves.

minimum value of 0.75, which indicates a relatively high degree of similarity between the two signals.

The stability of coupled delay differential equations has received substantial attention from researchers since the early 1970s. This problem can be addressed by using a Lyapunov-Krasovskii functional, a time domain methodology to investigate the stability properties of linear time-delay systems.[44] While a comprehensive stability analysis is not performed in this work, an observation may be made. For our study, the perturbation-based solution behaves in more stable way than the numerical benchmark. The latter did not work for time steps longer than 0.1 ms., while the former ran for time steps as long as 2 ms. An extension of this work should include a comprehensive analysis of the model stability, as a function of the time resolution, the physical parameters and the time delays.

## V.D   Perturbation - Data comparison

The perturbation-based solution was also tested again the data described in Section IV. The experimental impulse response, obtained by performing an inverse Fourier transform on the measured transfer function, was compared with the pressure impulse response calculated using Eq. (43). The differential volume $\nu(t)$ for each bubble was calculated as the solution of the coupled system (32) for $\epsilon = 1$, i.e. $\nu(t) = \phi(t) = \phi_0(t) + \phi_1(t) + \phi_2(t) + ...$, where $\nu(t)$ is a $2N \times 1$ vector, and $N$ is the number of bubbles. The total simulated time was

0.4 s, corresponding to two blocks of 0.2 *s*. For each block, it was necessary to calculate 200

functions to reach convergence. The physical bubble parameters used in the simulation were

previously described in Section V.A, and are summarized in Table III.

**Table III: Input parameters for Figure 10**

| Parameter | Symbol | Value |
| --- | --- | --- |
| Surface bubble radius | $a_0$ | 0.0468 m |
| Damping constant | $\beta$ | 10 1/s |
| Average bubble depth | z | 1.1 m |
| Theoretical resonance frequency | $f_0$ | 83 Hz |
| Number of bubbles in the cage | N | 14 |

The acoustic field described by Eqs. (32) assumes a free field, i.e. the acoustic field

in the receiver position is only due to the direct propagation from the bubbles and the in-

cident field, and not from boundary reflections. Scattering models are usually developed

for free field conditions, and subsequently incorporated as an input in propagation models.

A comprehensive sound propagation analysis would include sea surface and layered bottom

reflections, refraction effects and internal waves, among others. Even when it is not intended

to implement a full propagation model, it is necessary to include certain reflections to rep-

resent the variation in the peak amplitude registered by the different hydrophones. Figure

8 shows the frequency variation of the transfer function, for the hydrophones located at 8 m, 12 m and 16 m depth. This figure illustrates how the amplitude of the transfer function changes at different points in the water column. An interesting feature to note from Figure 8 is the downshift in the peak frequency by multiple scattering effects. According to Eq. (26), the individual resonance frequency should be around 80 Hz, while this figure shows the peak at 63 Hz. The peak frequency of the collective resonance of the bubble cloud typically shifts down to a lower frequency than that of an individual bubble, due to radiative coupling between the bubbles. The magnitude of this shift effect increases as the number of bubbles is increased, and the separation among them is reduced. This behavior has been well documented in literature for various systems of interacting resonators.[14;45;46]

In order to represent the peak amplitude variation shown in Figure 8, first and second order reflections from sea surface and ocean bottom were incorporated in the impulse response solution. The reflected signal is estimated by delaying the free-field response in time, according to the total propagation path for each case. For example, the path for the first-order sea surface reflection, will be equal to the average distance between the bubbles and the sea surface point $G$, plus the distance between this point and the receiver. $G$ is the point at which the incident wave strikes the reflecting surface, considering specular reflection. This is just a first approximation to include propagation effects in the hydrohone position, since reflections in sea surface are usually diffusive, and bottom reflections depend upon the
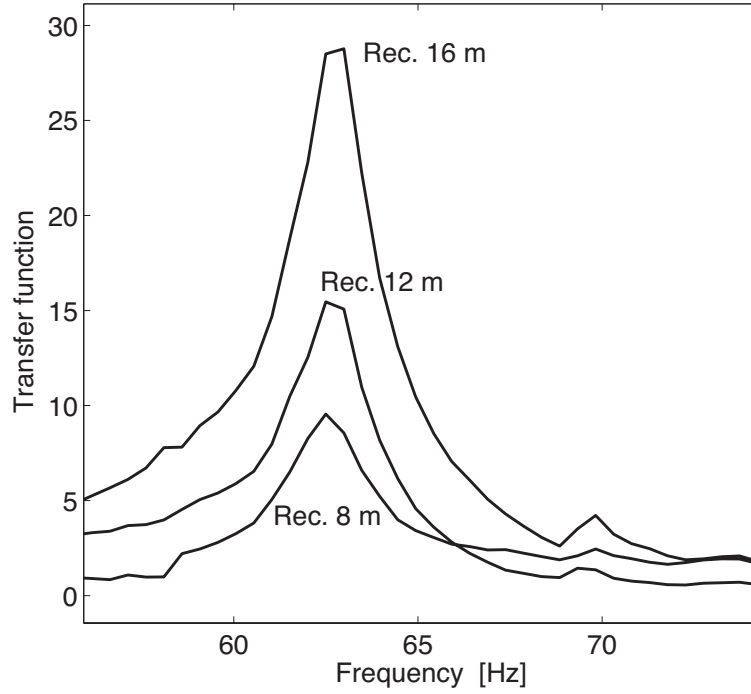
Figure 8: Variation of transfer function with frequency, for receivers located at 8 m, 12 m, and 16 m. depth.

seabed composition. Once the free-field impulse response is calculated, the total impulse response is estimated as:

$$\mathrm{IR}_{\mathrm{total}}(r,t) = \mathrm{IR}_{\mathrm{free}}(r,t) + \mathrm{R}_{\mathrm{B}}\mathrm{IR}_{\mathrm{free}}(r,t-t_{\mathrm{B}}) + \mathrm{R}_{\mathrm{S}}\mathrm{IR}_{\mathrm{free}}(r,t-t_{\mathrm{S}}),$$

$$+\mathrm{R}_{\mathrm{B}}\mathrm{R}_{\mathrm{S}}\mathrm{IR}_{\mathrm{free}}(r,t-t_{\mathrm{BS}}) + \mathrm{R}_{\mathrm{S}}\mathrm{R}_{\mathrm{B}}\mathrm{IR}_{\mathrm{free}}(r,t-t_{\mathrm{SB}}), \tag{47}$$

where $\mathrm{IR}_{\mathrm{free}}$ is the impulse response in free-field, and $\mathrm{R}_{\mathrm{B}}$, $\mathrm{R}_{\mathrm{S}}$ denote the reflection coefficient for the ocean bottom and sea surface (top boundary), respectively. Similarly, the subscripts

$B$ and $S$ in the time delays, stand for "bottom" and "surface" reflections. In expression

(47), each reflection is represented by a retarded function multiplied by a constant factor.

For example, $\mathrm{R_B IR_{free}}(r, t - t_\mathrm{B})$ designates the first order bottom reflection, where $t_\mathrm{B} = d_\mathrm{B}/c$ and $d_\mathrm{B}$ is the propagation distance for the first bottom reflection. Similarly, the term

$\mathrm{R_S R_B IR_{free}}(r, t - t_\mathrm{SB})$ denotes a second order reflection, where $t_\mathrm{SB} = d_\mathrm{SB}/c$ and $d_\mathrm{SB}$ is the

propagation distance for an incident wave hitting the sea surface and then the ocean bottom,

before reaching the receiver location.

The reflection on the ocean bottom depends upon the geoacoustic properties for the

seafloor and the grazing angle, i.e. the angle between the beam and the surface. The bottom

structure of Lake Travis consists of layers of unconsolidated mud, chalk/limestone and a very

hard layered limestone.[47] Using tabulated values of density and sound speed,[48] the reflection

coefficient was calculated using Rayleigh's expression for each receiver.[48] The estimated

average value of $R_\mathrm{B}$ is 0.62 for chalk, and 0.76 for limestone. Since Rayleigh's expression is

valid for a single interface, it is not possible to determine an effective reflection coefficient.

Also, the sea floor is covered by layers of sediments, which affects the amplitude and phase of

the reflected beam. However, it is expected that the average value of $R_\mathrm{B}$ is near 0.62 - 0.76.

On the other hand, the reflection from the sea surface is even harder to determine, since it

is also frequency dependent and sensitive to the surface roughness.[48] What we do know is

that the water/air interface, approached from the water side, is called a "pressure-release"

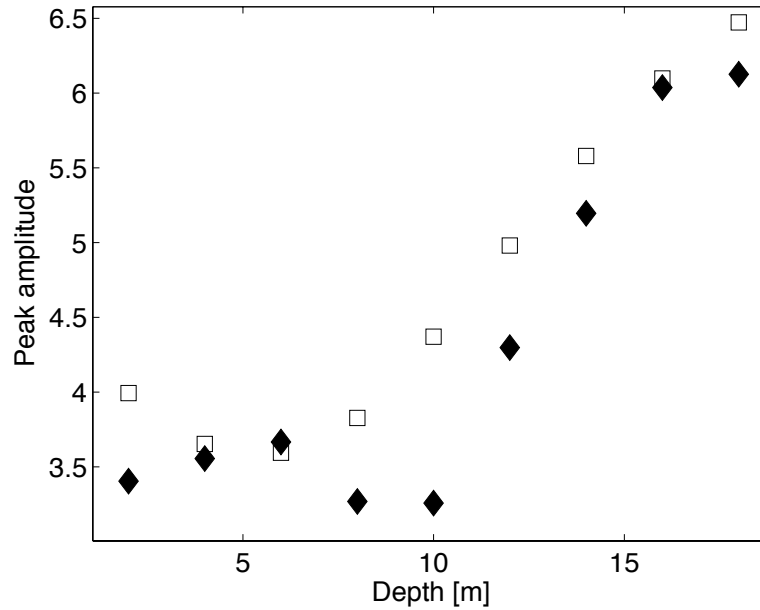surface for underwater sound, and the reflected pressure is phase-reversed.[49]



Figure 9: Transfer function peak amplitudes for all the nine receivers in the water column. $R_B = 0.7$ and $R_T = -0.1$. Note that $R_T$ is phase-reversed. Model:($\square$), Data:($\blacklozenge$).

The coefficients $R_B$ and $R_S$ were found by matching the peak amplitudes for the experimental and modeled transfer function. The latter was estimated by performing the Fourier transform of the calculated impulse response, including the reflections (Eq. 47). Although $R_B$ and $R_S$ depend upon the grazing angle, a single value was chosen for all the nine receivers. Future work may include angular and frequency dependent coefficients. Figure 9 shows the best match for the peak amplitudes, when $R_B = 0.7$ and $R_S = -0.1$. According

to the literature, the reflection coefficient for a flat pressure-release surface should be close to $R_S = -1.0$. However, the barge from which the experiment was conducted was floating on the surface on the water, therefore part of the reflection is coming from the bottom of the barge, which consist of metal containers filled with foam to provide flotation. The value of $R_S = -0.1$ found by matching the peak amplitudes indicated that the average reflection coefficient under the barge is still negative, but with absolute value less than unity.
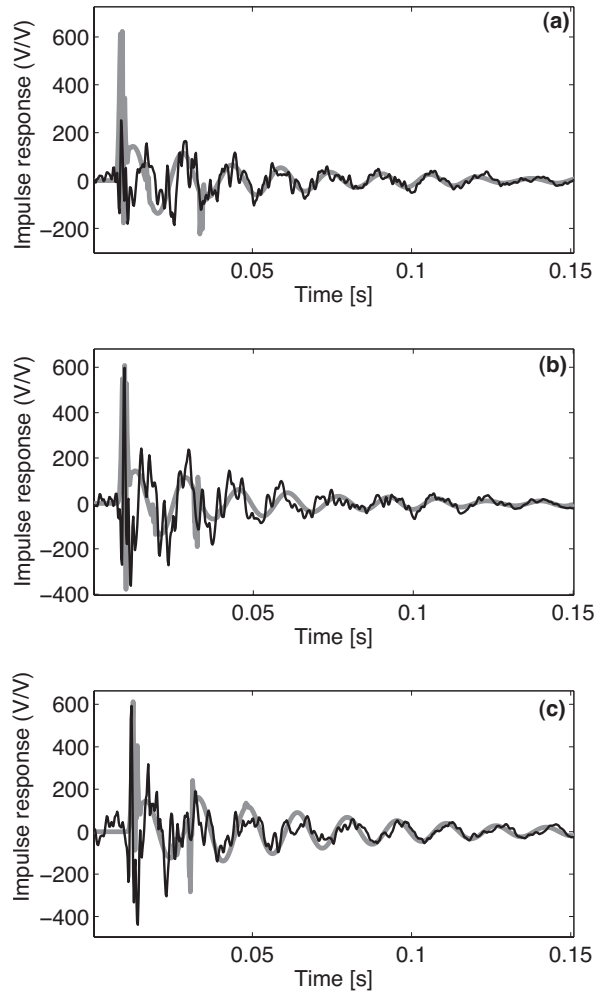
Figure 10: Pressure impulse response due to the bubbles, for the receivers located at (a)2 m, (b)6 m and (c)12 m depth. Black line: IFFT of transfer function data. Gray line: perturbation-based solution.

Figure 10 shows the pressure impulse response of the bubble system, for the receivers located at 2 m, 6 m and 12 m depth. The results for the remaining receivers are similar to the cases shown here, and therefore will be omitted. Each experimental curve was obtained by performing an inverse Fourier transform on the corresponding measured transfer function, after the phase adjustment described in Section IV. For all the three cases, the measured data shows a fundamental frequency that is very similar to the modeled fundamental frequency, as well as other transient features that match between measurements and model. Figure 10 also shows a good agreement for the general amplitude, as it is expected from Figure 9. In addition, the measured data shows some other higher frequency components, superimposed with the fundamental frequency, that are not present in the model and may be caused by boundary reflections.

# VI  Summary and Conclusions

This work presented a new method to calculate the impulse response of a near surface bubble cloud in a compressible medium and in the presence of a reflective bottom, based on the perturbation theory. The solution $\phi$ for the differential volume of each bubble is formulated as an expansion in a parameter $\epsilon$, where the first term of the expansion ($\phi_0$) corresponds to the solution of an exactly solvable problem. The remaining terms are iteratively calculated

and incorporate multiple scattering effects between bubbles. As the operators are defined, a value of ($\epsilon = 1$) is used in this work. Therefore, there is no reason to truncate the expansion, and a convergence criterion is needed. For this work, convergence was reached when the relative error between $\phi_n$ and $\phi_{n+1}$ was less than a tolerance value. In general, the convergence of the expansion will be determined by the physical bubble parameters and the interaction between them. It is important to note that the convergence is very sensitive to the interaction force, which depends upon the distance among scatterers. For a dense bubble cloud, the expansion will require more terms to converge.

The perturbation-based model was tested against experimental measurements of an artificial bubble cloud located near the surface of a shallow fresh water lake environment. The artificial bubble cloud consisted of 14 fixed latex balloons of 4.68 cm radius at the surface. Transfer functions (hydrophone voltage normalized by drive signal voltage) were measured from 30 Hz to 2 kHz by nine hydrophones, located at 2 meter intervals of depth from 2 meters to 18 meters, at a horizontal distance of 11.7 meters from the center of the bubble cloud. A measurement technique was used to isolate the acoustic effect of the bubble cloud scattering, by subtracting the signal due to the direct field (in the absence of a bubbles) from the signal arising from the bubble cloud. After the subtraction, nine different responses were found, corresponding to the nine receivers. The model shows good agreement with the experimentally measured transfer function data, both in amplitude and frequency. First and

second order boundary reflections were successfully incorporated to represent the variation in the peak amplitude registered by the different hydrophones.

A numerical benchmark was also implemented, using a fourth order Runge-Kutta algorithm. The input consisted in the impulse signal coming from the source and the multiple scattering among the bubbles. Two issues arise with the benchmark solution. The first one is the impulse implementation, which depends upon the impulsive function chosen. In the perturbation-based solution, the impulsive input is applied just to the soluble case (i.e., the first term of the expansion $\phi_0$), which can be solved analytically. Therefore, in this case there is no need to create an impulse function to solve the equation. The second issue is related to the stability. For the tested case, the numerical benchmark was less stable than the perturbation-based solution. Future work will explore the model stability as a function of the time resolution, system parameters, and time delays.

## Acknowledgements

## REFERENCES

1. P. D. Thorne and D. M. Hanes, "A review of acoustic measurement of small-scale sediment processes," Cont. Shelf. Res., **22**, 603–632, (2002).

2. P.G. Fernandes, F. Gerlotto, D. V. Holliday, O. Nakken, and E.J. Simmonds, "Acoustic applications in fisheries science: the ICES contribution," ICES Marine Science Symposia **215**, 483–492, (2002).

3. G. B. Farquhar, "Biological sound scattering in the oceans: a review," in *Oceanic Sound Scattering Prediction*, edited by N. R. Andersen and B. J. Zahuranec (Plenum, New York, 1977), pp. 493–527.

4. N. B. Marshall, "Bathypelagic fishes as sound scatterers in the ocean", J. Mar. Res. **10**, 1–17 (1951).

5. R.H. Love, C.H. Thompson, and R.W. Nero. "Changes in volume reverberation from deep to shallow water in the eastern Gulf of Mexico," J. Acoust. Soc. Am. **114**, 2698–2708 (2003)

6. L.L. Foldy, "The multiple scattering of waves. I. General theory of isotropic scattering by randomly distributed scatterers," Phys. Rev. **67**, 107–119 (1945).

7.  E.L. Carstensen and L.L. Foldy, "Propagation of sound through a liquid containing bubbles," J. Acoust. Soc. Am. **19**, 481–501 (1947).

8.  K.W. Commander and A. Prosperetti, "Linear pressure waves in bubbly liquids: Comparison between theory and experiments," J. Acoust. Soc. Am. **85**, 732–746 (1989).

9.  C. Feuillade, "The attenuation and dispersion of sound in water containing multiply interacting air bubbles," J. Acoust. Soc. Am. **99**, 3412–3430 (1996).

10. Z. Ye and L. Ding, "Acoustic dispersion and attenuation relations in bubbly mixture," J. Acoust. Soc. Am. **98**, 1629–1636 (1995).

11. S.G. Kargl, "Effective medium approach to linear acoustics in bubbly liquids," J. Acoust. Soc. Am. **111**, 168–173 (2002).

12. F.S. Henyey, "Corrections to Foldy's effective medium theory for propagation in bubble clouds and other collections of very small scatterers," J. Acoust. Soc. Am. **105**, 2149–2154 (1999).

13. E.A. Zabolotskaya, "Interaction of gas bubbles in a sound field," Sov. Phys. Acoust. **30**, 365–368 (1984).

14.  C. Feuillade, R.W. Nero and R.H. Love, "A low-frequency acoustic scattering model for small schools of fish," J. Acoust. Soc. Am. **99**, 196–208 (1996).

15.  T.G. Leighton, *The Acoustic Bubble* (Academic Press, San Diego, 1994).

16.  A.A. Doinikov and S.T. Zavtrak, "On the mutual interaction of two gas bubbles in a sound field," Phys. Fluids, **7**, 1923–1930 (1995).

17.  R. Mettin, I. Akhatov, U. Parlitz, C.D. Ohl, and W. Lauterborn, "Bjerknes forces between small cavitation bubbles in a strong acoustic field," Phys. Rev. E **56** 2924–2931 (1997).

18.  A.A. Doinikov and S.T. Zavtrak, "Radiation forces between two bubbles in a compressible liquid," J. Acoust. Soc. Am. **102**, 1424–1431 (1997).

19.  A.A. Doinikov, "Acoustic radiation interparticle forces in a compressible fluid," J. Fluid Mech. **444**, 1–21 (2001).

20.  R. Mettin, S. Luther, S. Kamphausen, and W. Lauterborn, "Dynamics of delay-coupled spherical bubbles," In AIP Conference Proceedings. IOP Institute of Physics Publishing LTD, (2000).

21.  C. Feuillade, "Acoustically coupled gas bubbles in fluids: Time domain phenomena," J. Acoust. Soc. Am. **109**, 2606–2615 (2001).

22. P.-Y. Hsiao, M. Devaud, and J.-C. Bacri, "Acoustic coupling between two air bubbles in water," The European Physical Journal E, **4**, 5–10 (2001).

23. A.A. Doinikov, R. Manasseh, and A. Ooi, "Time delays in coupled multibubble systems," J. Acoust. Soc. Am. **117**, 47–50 (2005).

24. A. Ooi, A. Nikolovska, and R. Manasseh, "Analysis of time delay effects on a linear bubble chain system," J. Acoust. Soc. Am. **124**, 815–826 (2008).

25. W.D. McComb, *Renormalization Methods: A Guide for Beginners*, pages 28–33. Oxford University Press, 2004.

26. M. Minnaert, "On musical air-bubbles and the sounds of running water," The London, Edinburgh,and Dublin Philosophical Magazine and Journal of Science: Series 7 **16**, 235–248 (1933).

27. C. Devin,"Survey of thermal, radiation, and viscous damping of pulsating air bubbles in water," J. Acoust. Soc. Am. **31**, 1654–1667 (1959).

28. H.Y. Hu, E.H. Dowell, and L.N. Virgin, "Stability estimation of high dimensional vibrating systems under state delay feedback control," J. Sound Vib. , **214**, 497–511 (1998).

29. C.C. Church, "The effects of an elastic solid surface layer on the radial pulsations of gas bubbles," J. Acoust. Soc. Am. **97**, 1510–1521 (1995).

30. A. Prosperetti, "Thermal effects and damping mechanisms in the forced radial oscillations of gas bubbles in liquids," J. Acoust. Soc. Am. **61**, 17–27 (1977).

31. K. Ogata, *System Dynamics*, Chapters 5.1 and 8.5. Pearson Education, fourth edition, (2004).

32. C.-T. Chen, *Linear System Theory and Design*, Oxford University Press, third edition, (1999).

33. C. Dolder, Direct Measurement of Effective Medium Properties of Model Fish Schools. PhD thesis, The University of Texas at Austin, (2014). Available: `https://repositories.lib.utexas.edu/handle/2152/24798`. [Accessed: 15-Feb-2017]

34. G. Enenstein, Two studies on the acoustics of multiphase materials: Seagrass tissue and encapsulated bubbles. Masters thesis, The University of Texas at Austin, (2014). Available: `https://repositories.lib.utexas.edu/handle/2152/26321`. [Accessed: 15-Feb-2017]

35. T.G. Leighton, P.R. White, C.L. Morfey, J.W.L. Clarke, G.J. Heald, H.A. Dumbrell

and K.R. Holland, "The effect of reverberation on the damping of bubbles," J. Acoust. Soc. Am. **112**, 1366–1376 (2002).

36. A.P. French, *Vibration and Waves*, chapter 4, pages 80–90. CRC press, (1971).

37. L. Guillon, C.W. Holland, and C. Barber, "Crossspectral analysis of midfrequency acoustic waves reflected by the seafloor," IEEE J. Oceanic Eng., **36**, 248–258 (2011).

38. K.M. Lee, A.R. McNeese, L.M. Tseng, M.S. Wochner, and P.S. Wilson, "Measurements of resonance frequencies and damping of large encapsulated bubbles in a closed, water-filled tank," In Proceedings of Meetings on Acoustics, volume 18. Acoustical Society of America, (2012).

39. R.N. Capps, Elastomeric materials for acoustical applications. Technical Report AD-A216872, Naval Research Laboratory. Available: `http://www.dtic.mil/dtic/tr/fulltext/u2/a216872.pdf`. [Accessed: 10-Jan-2017]

40. H. Lamb, *Hydrodynamics*, 6th ed. (Dover, New York, 1945), Sec. 56.

41. S. Hassani, *Mathematical Physics: A Modern Introduction to its Foundations*, Springer Science and Business Media (2013).

42. G.C. Carter, C.H. Knapp, and A.H. Nuttall, "Estimation of the magnitude-squared

coherence function via overlapped fast Fourier transform processing," Audio and Electroacoustics, IEEE Transactions **2**1, 337–344 (1973).

43. P.D. Welch, "The use of fast Fourier transform for the estimation of power spectra: A method based on time averaging over short, modified periodograms," IEEE Transactions on audio and electroacoustics **15**, 70–73 (1967).

44. A. Papachristodoulou, M. Peet, and S. Lall. "Constructing Lyapunov-Krasovskii functionals for linear time delay systems," American Control Conference, 2005. Proceedings of the 2005, IEEE, 2845–2850, (2005).

45. V. Twersky, "Multiple scattering of waves and optical phenomena," JOSA, **52**, 145–169, (1962).

46. D.E. Weston, "Acoustic interaction effects in arrays of small spheres," J. Acoust. Soc. Am. **39**, 316–322 (1966).

47. S.A. Stotts, D.P. Knobles, J.A. Keller, J.N. Piper and L.A. Thompson, "Geoacoustic inversion of short range source data using a plane wave reflection coefficient approach," J. Acoust. Soc. Am. **120**, 3607–3626 (2006).

48. J.H. Steele, S.A. Thorpe, and K.K. Turekian, *Elements of Physical Oceanography: A Derivative of the Encyclopedia of Ocean Sciences.* Academic Press, (2009).

**49.**   H. Medwin and C.S. Clay, *Fundamentals of Acoustical Oceanography* (Academic Press, Boston, 1998), pp. 237–238.